EARTHQUAKE ENGINEERING AND STRUCTURAL DYNAMICS, VOL. 25, 561–583 (1996)

EFFECT OF SLAB FLEXIBILITY ON INTERACTION BETWEEN TWO CIRCULAR FOUNDATIONS

GIN-SHOW LIOU*

Department of Civil Engineering, National Chiao-Tung University, 1001 Ta Hsueh Road, Hsin-Chu, Taiwan 30049

SUMMARY

The paper is aimed at investigating the effect of foundation rigidity on dynamic stiffness for two circular foundations on a viscoelastic medium. To generate the dynamic stiffness, a substructure technique is employed. For the substructure of a viscoelastic medium, the solution for wave motion reported in Reference 11 is used. For the substructures of two flexible foundations, classical plate theory with the inertial force neglected is employed to find the displacement fields of the foundation plates subjected to the interaction stresses. Then, the continuity condition for all the substructures is imposed implicitly by using the variational principle; then with the help of the reciprocal theorem the dynamic stiffness for the two flexible foundations can be obtained. For the numerical study, the boundary condition at the rims of both foundation plates is assumed to be a hinge connection to superstructures. Some numerical investigations are performed and the effect of foundation rigidity on dynamic stiffness is examined. Some discussions and conclusions are also made.

KEY WORDS: dynamic stiffness matrix; soil–structure interaction; structure-to-structure interaction; analytic solution; substructure technique

INTRODUCTION

In recent decades, structure–soil–structure interaction has started to draw much attention of many researchers in the field of earthquake engineering, since some massive and important structures may be constructed close together; for example: confinement structures of nuclear reactors of power plant and huge oil storage tanks. To perform the analysis of the interaction, a substructure technique is conventionally employed, in which the soil medium can be represented by dynamic stiffness matrices for structure foundations and then these matrices are incorporated into the total stiffness matrix of the superstructure for dynamic analysis of the structure–soil–structure system. Therefore, finding dynamic stiffness matrices is an essential step for this kind of interaction analysis.

Some research effort has been devoted to generate the dynamic stiffness matrices for multiple foundation systems. Warburton *et al.*[1] employed the solution for a single foundation to approximate the displacement at the second foundation through an averaging process and then to calculate the dynamic stiffness functions. Savidis and Richter[2] employed Green's function for a half-space to generate the boundary integral equation for a two-foundation system. Wang and Luco[3] extended a similar idea to generate the boundary integral equation for multiple foundation systems. Triantafyllidis and Prange[4] employed influence functions (integral of Green's function) to generate the dynamic stiffness functions for a two-foundation system. Lin *et al.*[5] employed hybrid modelling, in which the near field of the soil medium is modelled by the finite element method and the complementary far field of the soil medium is simulated by the consistent boundary method, to study the behaviour of vibrations of two embedded foundations. Also, Kawakami and Tasaki[6] used the boundary element technique to develop a simplified procedure to investigate the interaction effect of two masses excited by wave motion in a half-space medium.

*Professor

CCC 0098–8847/96/060561–23

Received 21 January 1995
Revised 28 December 1995

However, all the methods mentioned above are focused on the interaction of rigid foundations. When foundations are not rigid enough, the flexibility of the foundations will influence greatly the dynamic stiffness, which represents the rigidity of the surrounding soil medium, for the foundations themself as reported in many publications for the case of a single foundation; for example: Krenk and Schmidt[7] in 1981, Iguchi and Luco[8] in 1982, Rajapakse[9] in 1989 and Liou and Huang[10] in 1994. Therefore this paper is devoted to investigate the effect of foundation flexibility on dynamic stiffness matrices for a two-foundation system.

To generate dynamic stiffness matrices for two circular flexible foundations, the substructure technique is employed. For the substructure of a viscoelastic half-space medium or layered medium, the procedure reported in Reference 11, in which the interaction of two rigid circular foundations is considered, is used to obtain the solution of wave motion in the media due to application of interaction stresses. For substructures of flexible foundation plates, classical plate theory with inertial force and in-plane deformation neglected is employed to obtain the flexural deformations of the foundation plates subjected to interaction stresses. Then the compatibility condition for displacement is implicitly imposed by using the variational principle. After this, the dynamic stiffness matrices for the two foundations are generated by employing the reciprocal theorem.

Theoretically, an infinite number of Fourier components with respect to azimuth should be involved in the calculation of dynamic stiffness matrices, since the system with two separate circular foundations is no longer axially symmetric. Numerically, this is impossible. Therefore, the required number of Fourier components for obtaining accurate results is investigated first in the paper. Then some selected numerical results for two foundations are presented and the effect of foundation rigidity is examined. Discussions and conclusions of the effect of foundation rigidity are also made in the paper.

ANALYSIS PROCEDURE

For generating dynamic stiffness matrices for two flexible circular foundations on a viscoelastic soil medium, the motion of the total system is assumed to be harmonic with respect to time. For convenience and simplicity, the time harmonic term $e^{i\omega t}$ will be omitted in the following derivations and expressions. The substructure technique is employed to generate the dynamic stiffness matrices. The total system is divided into three substructures: one is the viscoelastic medium and the other two are the two flexible foundations. The interaction stresses between the foundation plate and the viscoelastic medium can be decomposed into an infinite Fourier series with respect to azimuth. For each Fourier component of the interaction stresses, the distribution in the r-direction of the cylindrical co-ordinates is assumed to be piecewise linear. Therefore, the interaction stress vectors ($[\tau_{rz}, \sigma_{zz}, \tau_{\theta z}]^T$) for foundation No. 1 and No. 2 shown in Figure 1 can be expressed as follows:

$$\mathbf{t}_1(r_1, \theta_1) = \sum_{n=0}^{\infty} (\mathbf{L}_n^s \mathbf{H}_1^T \mathbf{P}_{1,n}^s + \mathbf{L}_n^a \mathbf{H}_1^T \mathbf{P}_{1,n}^a) \tag{1}$$

$$\mathbf{t}_2(r_2, \theta_2) = \sum_{m=0}^{\infty} (\mathbf{L}_m^s \mathbf{H}_2^T \mathbf{P}_{2,m}^s + \mathbf{L}_m^a \mathbf{H}_2^T \mathbf{P}_{2,m}^a) \tag{2}$$

where the 3×3 diagonal circumferential variation matrices L's can be written as $\mathrm{diag}(\cos n\theta_i, \cos n\theta_i, -\sin n\theta_i)$ or $\mathrm{diag}(\sin n\theta_i, \sin n\theta_i, \cos n\theta_i)$ in which i can be 1 or 2, and the piecewise linear distribution matrices $\mathbf{H}_1$ and $\mathbf{H}_2$ are defined by equations (30) and (31) in the Appendix, and vectors **P**'s are the stress intensity vectors for the stress intensities at the locations of nodal rings in the assumed piecewise linear stress model and are also defined by equations (30) and (31) in the Appendix. In the equations above and the equations thereafter, the subscripts n and m represent Fourier component numbers for foundation No.1 and No. 2 respectively, superscript T represents transpose of a matrix, and superscripts s and a represent respectively symmetric and anti-symmetric with respect to the line connecting the centres of two cylindrical co-ordinate systems for the two circular foundations.

For the substructure of the viscoelastic medium subjected to the tractions $\mathbf{t}_1$ and $\mathbf{t}_2$ in equations (1) and (2), the displacement fields $\mathbf{u}_1$ (for $\mathbf{t}_1$) and $\mathbf{u}_2$ (for $\mathbf{t}_2$) can be obtained using the procedure described in

Reference 11. After some manipulations, the displacement fields $\mathbf{u}_1$ and $\mathbf{u}_2$ can be written respectively as follows:

$$\mathbf{u}_1(r_1, \theta_1) = \sum_{n=0}^{\infty} \left(\mathbf{L}_n^s \int_0^{\infty} \mathbf{J}_n \mathbf{Q} \bar{\mathbf{D}}_n \mathbf{P}_{1,n}^s \, dk_1 + \mathbf{L}_n^a \int_0^{\infty} \mathbf{J}_n \mathbf{Q} \bar{\mathbf{D}}_n \mathbf{P}_{1,n}^a \, dk_1 \right) \tag{3}$$

and

$$\mathbf{u}_2(r_2, \theta_2) = \sum_{m=0}^{\infty} \left(\mathbf{L}_m^s \int_0^{\infty} \bar{\mathbf{J}}_m \bar{\mathbf{Q}} \bar{\mathbf{D}}_m \mathbf{P}_{2,m}^s \, dk_2 + \mathbf{L}_m^a \int_0^{\infty} \bar{\mathbf{J}}_m \bar{\mathbf{Q}} \bar{\mathbf{D}}_m \mathbf{P}_{2,m}^a \, dk_2 \right) \tag{4}$$

in which matrices $\mathbf{J}_n, \mathbf{Q}, \bar{\mathbf{D}}_n$ are defined in the Appendix by equations (32)–(34) and matrices $\bar{\mathbf{J}}_m, \bar{\mathbf{Q}}, \bar{\mathbf{D}}_m$ can be similarly defined except the wave number k_1 and the $r_1 - \theta_1 - z_1$ co-ordinate system are replaced with k_2 and the $r_2 - \theta_2 - z_2$ co-ordinate system. Therefore, the total displacement field due to the application of $\mathbf{t}_1$ and $\mathbf{t}_2$ can be obtained by just adding equations (3) and (4) together: i.e.

$$\mathbf{u} = \mathbf{u}_1 + \mathbf{u}_2 \tag{5}$$

In the equation, one should note that $\mathbf{u}_1$ and $\mathbf{u}_2$ are expressed in different co-ordinate systems. Therefore, co-ordinate transformation between the two systems must be applied to either $\mathbf{u}_1$ or $\mathbf{u}_2$ in order to obtain a consistent system for $\mathbf{u}$. The co-ordinate transformation matrix can be written as

$$\mathbf{T} = \begin{bmatrix} \cos(\theta_2 - \theta_1) & 0 & -\sin(\theta_2 - \theta_1) \\ 0 & 1 & 0 \\ \sin(\theta_2 - \theta_1) & 0 & \cos(\theta_2 - \theta_1) \end{bmatrix} \tag{6}$$

Now, the variational principle can be applied for the substructure of the half-space medium with the prescribed traction $\mathbf{t}_1$ and $\mathbf{t}_2$ in equations (1) and (2). The work done by variations of $\mathbf{t}_1$ and $\mathbf{t}_2$ can be written as

$$\delta W = \int_0^{a_1} \int_0^{2\pi} \delta \mathbf{t}_1^{\mathrm{T}} (\mathbf{u}_1 + \mathbf{T}\mathbf{u}_2) r_1 \, d\theta_1 \, dr_1 + \int_0^{a_2} \int_0^{2\pi} \delta \mathbf{t}_2^{\mathrm{T}} (\mathbf{T}^{\mathrm{T}} \mathbf{u}_1 + \mathbf{u}_2) r_2 \, d\theta_2 \, dr_2 \tag{7}$$

where a_1 and a_2 are the radii of the two circular foundations. In order to perform numerical calculation, the infinite Fourier series of $\mathbf{t}_1$ and $\mathbf{t}_2$ must be truncated to a finite series. The accuracy of numerical results due to the truncations will be investigated later in the section of Numerical Results. After some mathematical manipulations,[11] the work done in equation (7) can be written as

$$\delta W = \begin{bmatrix} \delta \mathbf{P}^s \\ \delta \mathbf{P}^a \end{bmatrix}^{\mathrm{T}} \begin{bmatrix} \mathbf{K}^s & \mathbf{0} \\ \mathbf{0} & \mathbf{K}^a \end{bmatrix} \begin{bmatrix} \mathbf{P}^s \\ \mathbf{P}^a \end{bmatrix} \tag{8}$$

where

$$\mathbf{P}^{s^{\mathrm{T}}} = [\mathbf{P}_{1,1}^{s^{\mathrm{T}}} \cdots \mathbf{P}_{1,A}^{s^{\mathrm{T}}} \; \mathbf{P}_{2,1}^{s^{\mathrm{T}}} \cdots \mathbf{P}_{2,B}^{s^{\mathrm{T}}}] \tag{8a}$$

$$\mathbf{P}^{a^{\mathrm{T}}} = [\mathbf{P}_{1,1}^{a^{\mathrm{T}}} \cdots \mathbf{P}_{1,A}^{a^{\mathrm{T}}} \; \mathbf{P}_{2,1}^{a^{\mathrm{T}}} \cdots \mathbf{P}_{2,B}^{a^{\mathrm{T}}}] \tag{8b}$$

$$\mathbf{K}^s = \begin{bmatrix} \mathbf{K}_{11}^s & \mathbf{0} & \cdots & \mathbf{0} & \mathbf{K}_{1,1}^s & \cdots & \mathbf{K}_{1,B}^s \\ \mathbf{0} & \mathbf{K}_{22}^s & \cdots & \mathbf{0} & \mathbf{K}_{2,1}^s & \cdots & \mathbf{K}_{2,B}^s \\ \vdots & \vdots & \ddots & \vdots & \vdots & \ddots & \vdots \\ \mathbf{0} & \mathbf{0} & \cdots & \mathbf{K}_{A,A}^s & \mathbf{K}_{A,1}^s & \cdots & \mathbf{K}_{A,B}^s \\ \bar{\mathbf{K}}_{1,1}^s & \bar{\mathbf{K}}_{1,2}^s & \cdots & \bar{\mathbf{K}}_{1,A}^s & \bar{\mathbf{K}}_{11}^s & \cdots & \mathbf{0} \\ \vdots & \vdots & \vdots & \vdots & \vdots & \ddots & \vdots \\ \bar{\mathbf{K}}_{B,1}^s & \bar{\mathbf{K}}_{B,2}^s & \cdots & \bar{\mathbf{K}}_{B,A}^s & \mathbf{0} & \cdots & \bar{\mathbf{K}}_{BB}^s \end{bmatrix} \tag{8c}$$

the expression for $\mathbf{K}^a$ is similar to that for $\mathbf{K}^s$, the subscripts A and B represent the highest Fourier components for the truncated $\mathbf{t}_1$ and $\mathbf{t}_2$ respectively, and the submatrices in the matrices $\mathbf{K}^a$ and $\mathbf{K}^s$ are shown in equations (35)–(38) in the Appendix. In the equations above, the zero entries of the matrices are due to the orthogonal property of Fourier components. Also, the reciprocal theorem can be employed to demonstrate that $\mathbf{K}^s$ and $\mathbf{K}^a$ are symmetric matrices. All the above derivations for the substructure of a half-space medium can also be found in Reference 11 in more detail.

For the substructures of two circular foundations subjected to the interaction stresses defined in equations (1) and (2), classical plate theory with inertial force neglected is employed to obtain the flexural deformation of the substructures. Since the axial deformation of plates is also suppressed, only the second component σ_{zz} in the interaction stress vectors $\mathbf{t}_1$ and $\mathbf{t}_2$ is taken into account for obtaining foundation deformation. The governing equation of the foundation plate subjected to the loading of $\sigma_{zz,n}$, the nth Fourier component of σ_{zz}, can be written as

$$S\nabla^2\nabla^2 w_n(r) = \sigma_{rr,n}(r) \tag{9}$$

where

$$w_n(r) = u_{z,n}(r) - \Delta_{z,n}(r), \quad \nabla^2 = \frac{\partial^2}{\partial r^2} + \frac{1}{r}\frac{\partial}{\partial r} + \frac{n^2}{r^2} \tag{10}$$

$S = Eh^3/12(1-\nu^2)$ is the plate rigidity in which E is Young's modulus, h is the plate thickness and ν is Poisson's ratio, $\Delta_{z,n}(r)$ is the displacement due to rigid body motion which only exists for $n = 0$ and 1, and $u_{z,n}(r)$ is the total displacement for the nth Fourier component. For example: $\Delta_{z,0}(r) = \Delta_0$ for vertical motion ($n = 0$) and $\Delta_{z,1}(r) = \Delta_1 r$ for rocking or pitching motions of circular foundation ($n = 1$), in which Δ_0 and Δ_1 are amplitudes of the rigid body motions.

Since the loading $\sigma_{zz,n}(r)$ is arbitrary, there is no exact solution for equation (9). However, if one treats $\sigma_{zz,n}(r_p)\,dr_p$ as a concentrated loading applied at $r = r_p$ and divides the plate into an inner circular plate for $r < r_p$ and an outer annular plate for $r > r_p$, then the governing equation (equation (9)) becomes $S\nabla^2\nabla^2\,dw_{n,1}(r) = 0$ and $S\nabla^2\nabla^2\,dw_{n,2}(r) = 0$ for the inner plate and outer plate respectively. The solutions for these two equations can be easily found as follows:

$$dw_{n,1}(r) = F_n(r) \quad \text{for } r < r_p \tag{11}$$

$$dw_{n,2}(r) = f_n(r) \quad \text{for } r_p < r < a_0 \tag{12}$$

where

$$F_n(r) = C_{10} + C_{20}r^2 + C_{30}\ln(r) + C_{40}r^2\ln(r) \quad \text{for } n = 0 \tag{13}$$

$$F_n(r) = C_{11}r + C_{21}r^3 + C_{31}r^{-1} + C_{41}r\ln(r) \quad \text{for } n = 1 \tag{14}$$

$$F_n(r) = C_{1n}r^n + C_{2n}r^{-n} + C_{3n}r^{n+2} + C_{4n}r^{-n+2} \quad \text{for } n > 1 \tag{15}$$

and $f_n(r)$ has similar forms to equations (13)–(15). To determine the coefficients for $F_n(r)$ in equations (13)–(15) and $f_n(r)$, one can use the boundary condition at the rim of the whole plate, which could be hinged, clamped or free, and finite displacement and moment at $r = 0$, and the continuity of displacement and the equilibrium of total shear force with $\sigma_{zz,n}(r_p)\,dr_p$ at $r = r_p$. Therefore, these coefficients are also functions of r_p. The total deformation at an arbitrary r for the loading $\sigma_{zz,n}(r)$ can be obtained through superimposing the integrations of equations (11) and (12) with respect to r_p. This will lead to the following expression:

$$w_n(r) = [\mathbf{1}]^T\mathbf{R}_n(r)\mathbf{p}_n \tag{16}$$

where

$$\mathbf{R}_n(r) = \begin{bmatrix} R_{00,n}(r) & \cdots & R_{0l,n}(r) \\ \vdots & \ddots & \vdots \\ R_{l0,n}(r) & \cdots & R_{ll,n}(r) \end{bmatrix} \tag{17}$$

in which $R_{ij,n}(r)$ is the displacement at r locating between the $(i-1)$th nodal ring and the $(i+1)$th nodal ring due to the application of the loading with unit intensity at the jth nodal ring in the piecewise linear stress model in equations (1) or (2), vector $[\mathbf{1}] = (1, 1, \ldots, 1)^T$, and vector $\mathbf{p}_n$ is for the intensities at nodal rings for $\sigma_{zz,n}$.

For each of the two flexible foundations, the total displacement field for the nth Fourier component can be expressed as the composition of rigid body displacement and flexible deformation as follows:

$$\mathbf{u}_n = \mathbf{u}_n^r + \mathbf{u}_n^f = (u_{r,n}, u_{z,n}, u_{\theta,n})^T + (0, w_n, 0)^T \tag{18}$$

In the above derivation of foundation deformation, the circumferential variation of $\cos n\theta$ or $\sin n\theta$ for the nth Fourier component has been omitted for convenience and simplicity. One can also notice that there are three cases regarding the displacement of rigid body motion and flexural deformation of foundations in equation (18). These three cases are explained as follows: (1) When $n = 0$, $\mathbf{u}_0^r = (0, 0, r)^T\Delta_0^a$ and $\mathbf{u}_0^f = \mathbf{0}$ for torsional motion of the foundation and $\mathbf{u}_0^r = (0, 1, 0)^T\Delta_0^s$ for vertical motion. (2) When $n = 1$, $\mathbf{u}_1^r = (1, 0, 1)^T\Delta_{1,h} + (0, r, 0)^T\Delta_{1,r}$ for horizontal and rocking motions or horizontal and pitching motions. (3) When $n \geqslant 2$, $\mathbf{u}_n^r = 0$ always.

Now the variational principle can be employed again for the substructures of flexible foundations. Since the Fourier components for the case of circular foundations are orthogonal to each other, the virtual work done by variation of interaction stresses can be calculated independently for each Fourier component. This gives the following expressions for one component:

$$\delta W_n = \int_0^{a_0}\int_0^{2\pi} \delta\mathbf{t}_n^T\mathbf{u}_n r\,d\theta\,dr = \delta\mathbf{P}_n^T\mathbf{B}_n\Delta_n + \delta\mathbf{P}_n^T\mathbf{K}_{2,n}\mathbf{P}_n \tag{19}$$

$$\mathbf{K}_{2,n} = \begin{bmatrix} \mathbf{0} & \mathbf{0} & \mathbf{0} \\ \mathbf{0} & \bar{\mathbf{K}}_{2,n} & \mathbf{0} \\ \mathbf{0} & \mathbf{0} & \mathbf{0} \end{bmatrix}, \quad \bar{\mathbf{K}}_{2,n} = \begin{pmatrix} 2\pi \\ \pi \end{pmatrix} \int_0^{a_0} \mathbf{h}^T[\mathbf{1}]\mathbf{R}_n(r) r\,dr \tag{20}$$

in which vector $\mathbf{t}_n$ is the nth component in equations (1) or (2), Δ_n is the amplitude of rigid body motion as discussed for equation (18), matrix $\mathbf{B}_n$ is the contribution from work done by unit rigid body displacements, and matrix $\mathbf{h}^T$ is the submatrix of $\mathbf{H}_1^T$ or $\mathbf{H}_2^T$ in equations (1) or (2), which is for the second component $\sigma_{zz,n}$ only and also shown in equations (30) in the Appendix. In equations (20), the constants π and 2π come from the integrations $\int_0^{2\pi} \sin^2 n\theta\,d\theta$ or $\int_0^{2\pi} \cos^2 n\theta\,d\theta$ which are not explicitly expressed in the equations.

For the two flexible foundations alone, the total work done for all Fourier components involved in computation can be expressed as

$$\delta W = \sum^n \delta W_n = \begin{bmatrix} \delta\mathbf{P}^s \\ \delta\mathbf{P}^a \end{bmatrix}\left(\begin{bmatrix} \mathbf{B}^s & \mathbf{0} \\ \mathbf{0} & \mathbf{B}^a \end{bmatrix}\begin{bmatrix} \Delta^s \\ \Delta^a \end{bmatrix} + \begin{bmatrix} \mathbf{K}_2^s & \mathbf{0} \\ \mathbf{0} & \mathbf{K}_2^a \end{bmatrix}\begin{bmatrix} \mathbf{P}^s \\ \mathbf{P}^a \end{bmatrix}\right) \tag{21}$$

where matrices $\mathbf{B}^s$ and $\mathbf{B}^a$ are formed by matrix $\mathbf{B}_n$ defined in equation (19), Δ^s and Δ^a are vectors for amplitudes of rigid body motions, and matrices $\mathbf{K}_2^s$ and $\mathbf{K}_2^a$ are diagonally formed by matrix $\mathbf{K}_{2,n}$ in equations (20); e.g.

$$\mathbf{K}_2^s = \text{diag}(\mathbf{K}_{2,0}, \mathbf{K}_{2,1}, \ldots, \mathbf{K}_{2,n}, \ldots)$$

Equating equation (21) to equation (8), which implies the displacement continuity between soil medium and foundations, one can obtain the following equations:

$$\begin{bmatrix} \mathbf{K}^s - \mathbf{K}_2^s & \mathbf{0} \\ \mathbf{0} & \mathbf{K}^a - \mathbf{K}_2^a \end{bmatrix}\begin{bmatrix} \mathbf{P}^s \\ \mathbf{P}^a \end{bmatrix} = \begin{bmatrix} \mathbf{B}^s & \mathbf{0} \\ \mathbf{0} & \mathbf{B}^a \end{bmatrix}\begin{bmatrix} \Delta^s \\ \Delta^a \end{bmatrix} \tag{22}$$

or

$$\bar{\mathbf{K}}^s\mathbf{P}^s = \mathbf{B}^s\Delta^s \quad \text{and} \quad \bar{\mathbf{K}}^a\mathbf{P}^a = \mathbf{B}^a\Delta^a \tag{23}$$

or

$$\mathbf{V}^s = \mathbf{B}^s\Delta^s \quad \text{and} \quad \mathbf{V}^a = \mathbf{B}^a\Delta^a \tag{24}$$

where vectors $\mathbf{V}^s$ and $\mathbf{V}^a$ are the generalized displacements at the nodal rings of the assumed piecewise linear stress model. Equations (24) give the relationship between amplitudes of rigid body motions and generalized displacements at nodal rings. To obtain the relationship between amplitude of excitation forces of rigid body motions and intensities of interaction stresses at nodal rings, one can apply the reciprocal theorem. This gives

$$\mathbf{F}^s = \mathbf{B}^{s^T}\mathbf{P}^s \quad \text{and} \quad \mathbf{F}^a = \mathbf{B}^{a^T}\mathbf{P}^a \tag{25}$$

where vectors $\mathbf{F}^s$ and $\mathbf{F}^a$ are generalized force amplitudes for rigid body motions. Substituting $\mathbf{P}^s$ and $\mathbf{P}^a$ from equations (23) into equations (25), the following equations are obtained:

$$\mathbf{F}^s = \mathbf{B}^{s^T}\bar{\mathbf{K}}^{s^{-1}}\mathbf{B}^s\Delta^s = \mathbf{I}^s\Delta^s \quad \text{and} \quad \mathbf{F}^a = \mathbf{B}^{a^T}\bar{\mathbf{K}}^{a^{-1}}\mathbf{B}^a\Delta^a = \mathbf{I}^a\Delta^a \tag{26}$$

where matrices $\mathbf{I}^s$ and $\mathbf{I}^a$ respectively are dynamic stiffness matrices for the symmetric and anti-symmetric motions with respect to the line connecting two centres of the two flexible foundations. The matrices $\mathbf{I}^s$ and $\mathbf{I}^a$ can be expressed as

$$\mathbf{I}^s = \begin{bmatrix} I_{v_1v_1} & I_{v_1R_1} & I_{v_1x_1} & I_{v_1v_2} & I_{v_1R_2} & I_{v_1x_2} \\ I_{R_1v_1} & I_{R_1R_1} & I_{R_1x_1} & I_{R_1v_2} & I_{R_1R_2} & I_{R_1x_2} \\ I_{x_1v_1} & I_{x_1R_1} & I_{x_1x_1} & I_{x_1v_2} & I_{x_1R_2} & I_{x_1x_2} \\ I_{v_2v_1} & I_{v_2R_1} & I_{v_2x_1} & I_{v_2v_2} & I_{v_2R_2} & I_{v_2x_2} \\ I_{R_2v_1} & I_{R_2R_1} & I_{R_2x_1} & I_{R_2v_2} & I_{R_2R_2} & I_{R_2x_2} \\ I_{x_2v_1} & I_{x_2R_1} & I_{x_2x_1} & I_{x_2v_2} & I_{x_2R_2} & I_{x_2x_2} \end{bmatrix} \tag{27}$$

and

$$\mathbf{I}^a = \begin{bmatrix} I_{T_1T_1} & I_{T_1p_1} & I_{T_1y_1} & I_{T_1T_2} & I_{T_1p_2} & I_{T_1y_2} \\ I_{p_1T_1} & I_{p_1p_1} & I_{p_1y_1} & I_{p_1T_2} & I_{p_1p_2} & I_{p_1y_2} \\ I_{y_1T_1} & I_{y_1p_1} & I_{y_1y_1} & I_{y_1T_2} & I_{y_1p_2} & I_{y_1y_2} \\ I_{T_2T_1} & I_{T_2p_1} & I_{T_2y_1} & I_{T_2T_2} & I_{T_2p_2} & I_{T_2y_2} \\ I_{p_2T_1} & I_{p_2p_1} & I_{p_2y_1} & I_{p_2T_2} & I_{p_2p_2} & I_{p_2y_2} \\ I_{y_2T_1} & I_{y_2p_1} & I_{y_2y_1} & I_{y_2T_2} & I_{y_2p_2} & I_{y_2y_2} \end{bmatrix} \tag{28}$$

In the subscripts of the equations, v represents vertical motion, R and p represent rocking and pitching motions respectively, T represents torsional motion, and x and y represent horizontal motions in the x and y directions. The directions of these motions can also be referred to Figure 1.

NUMERICAL RESULTS

Two identical flexible foundations with thin walled cylinders connecting to their rims are used to demonstrate the effect of foundation rigidity on dynamic stiffness matrices. Since the foundations are connected to superstructures through thin walled cylinders which only have little constraint of rotation at the rims, the boundary condition for the foundation plates is therefore assumed to be hinged. The two foundations are rigidly attached to a viscoelastic half-space medium and subjected to excitations in all possible directions by the thin walled cylinders. The directions of motions of the foundations and the co-ordinate systems are defined in Figure 1. For the half-space medium, the hysteretic damping ratio (ξ) is selected to be 0·05 with complex shear modulus $G = G_R(1 + 2\xi i)$ and Poisson's ratio is assumed to be 0·33. In order to study the effect of foundation rigidity, seven non-dimensional relative foundation stiffness parameters are selected and the parameter is defined as

$$\alpha = \frac{S}{G_R a_0^3} \tag{29}$$

in which S is the plate rigidity as shown in equation (9) and a_0 is the radius of the foundations. The seven α's are $\infty, 10, 5, 1, 0{\cdot}1, 0{\cdot}05, 0{\cdot}01$. Also, the effect of the separation distance of the two flexible foundations is presented. All numerical results presented in the paper are non-dimensionalized with the aid of the complex shear modulus (G) and the radius of the two identical foundations (a_0).

Theoretically, the number of Fourier components involved in the calculation of dynamic stiffness matrices for the two foundations should be infinite. However, one can truncate numerically Fourier components without losing accuracy. Therefore, the question of how many components are enough for obtaining fair results has to be answered first. Tables I–VI show some selected results with increasing the number of Fourier components used in the calculation for the case $d/a_0 = 0{\cdot}25$ in which d is the clear distance between the two foundations as shown in Figure 1. In Tables I–III, the results for non-dimensional vertical dynamic stiffnesses are presented for non-dimensional frequencies $\omega a_0/\mathrm{Re}(c_s)$ ($\mathrm{Re}(c_s)$ is the real part of the complex shear wave velocity) between 0·014273 and 10·2509 and non-dimensional foundation stiffness parameter α between 0·01

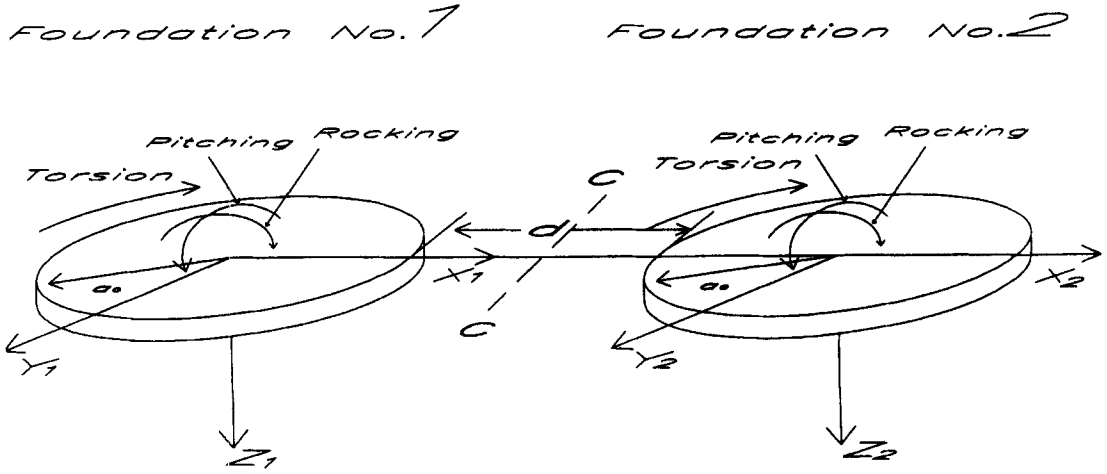

Figure 1. Definition of the motion of two foundations

Table I. Non-dimensional vertical dynamic stiffness for $\alpha = 10$ ($d/a_0 = 0{\cdot}25$)

n, m	$\frac{\omega a_0}{\mathrm{Re}(c_s)} = 0{\cdot}014273$	$\frac{\omega a_0}{\mathrm{Re}(c_s)} = 4{\cdot}2819$	$\frac{\omega a_0}{\mathrm{Re}(c_s)} = 10{\cdot}2509$
$\leqslant 1$	6·9034 + 0·03883i	5·7454 + 26·9315i	11·1289 + 63·1221i
$\leqslant 2$	6·9359 + 0·03895i	5·8230 + 26·9077i	11·0951 + 63·1315i
$\leqslant 3$	6·9527 + 0·03716i	5·7811 + 27·0539i	11·0883 + 63·0932i
$\leqslant 4$	6·9543 + 0·03716i	5·6861 + 26·9954i	11·0812 + 63·0979i

Table II. Non-dimensional vertical dynamic stiffness for $\alpha = 1$ ($d/a_0 = 0{\cdot}25$)

n, m	$\frac{\omega a_0}{\mathrm{Re}(c_s)} = 0{\cdot}014273$	$\frac{\omega a_0}{\mathrm{Re}(c_s)} = 4{\cdot}2819$	$\frac{\omega a_0}{\mathrm{Re}(c_s)} = 10{\cdot}2509$
$\leqslant 1$	6·7215 + 0·02149i	12·1743 + 25·7856i	30·1107 + 42·4969i
$\leqslant 2$	6·7526 + 0·02151i	12·2232 + 25·7687i	30·0821 + 42·5008i
$\leqslant 3$	6·7688 + 0·01972i	12·2038 + 25·8996i	30·0818 + 42·4688i
$\leqslant 4$	6·7704 + 0·01972i	12·1330 + 25·8367i	30·0743 + 42·4726i

Table III. Non-dimensional vertical dynamic stiffness for $\alpha = 0{\cdot}01$ ($d/a_0 = 0{\cdot}25$)

n, m	$\frac{\omega a_0}{\mathrm{Re}(c_s)} = 0{\cdot}014273$	$\frac{\omega a_0}{\mathrm{Re}(c_s)} = 4{\cdot}2819$	$\frac{\omega a_0}{\mathrm{Re}(c_s)} = 10{\cdot}2509$
$\leqslant 1$	5·0324 − 0·00403i	6·1473 + 4·5433i	9·6579 + 8·9159i
$\leqslant 2$	5·0514 − 0·00420i	6·1905 + 4·5850i	9·6454 + 8·9072i
$\leqslant 3$	5·0621 − 0·00549i	6·0819 + 4·6039i	9·6640 + 8·8905i
$\leqslant 4$	5·0631 − 0·00551i	6·0834 + 4·5276i	9·6594 + 8·8943i

Table IV. Non-dimensional pitching dynamic stiffness for $\alpha = 10$ ($d/a_0 = 0{\cdot}25$)

n, m	$\frac{\omega a_0}{\mathrm{Re}(c_s)} = 0{\cdot}014273$	$\frac{\omega a_0}{\mathrm{Re}(c_s)} = 4{\cdot}2819$	$\frac{\omega a_0}{\mathrm{Re}(c_s)} = 10{\cdot}2509$
$\leqslant 1$	4·1058 + 0·00001i	2·0220 + 5·9097i	2·9337 + 15·5496i
$\leqslant 2$	4·1107 + 0·00001i	2·0162 + 5·9072i	2·9341 + 15·5496i
$\leqslant 3$	4·1127 + 0·00001i	2·0313 + 5·8938i	2·9338 + 15·5506i
$\leqslant 4$	4·1134 + 0i	2·0403 + 5·9148i	2·9339 + 15·5506i

Table V. Non-dimensional pitching dynamic stiffness for $\alpha = 1$ ($d/a_0 = 0{\cdot}25$)

n, m	$\frac{\omega a_0}{\mathrm{Re}(c_s)} = 0{\cdot}014273$	$\frac{\omega a_0}{\mathrm{Re}(c_s)} = 4{\cdot}2819$	$\frac{\omega a_0}{\mathrm{Re}(c_s)} = 10{\cdot}2509$
$\leqslant 1$	4·0852 − 0·00200i	2·1093 + 5·9480i	3·8569 + 15·4273i
$\leqslant 2$	4·0900 − 0·00200i	2·1035 + 5·9458i	3·8573 + 15·4273i
$\leqslant 3$	4·0920 − 0·00201i	2·1179 + 5·9319i	3·8569 + 15·4283i
$\leqslant 4$	4·0927 − 0·00201i	2·1274 + 5·9524i	3·8570 + 15·4283i

Table VI. Non-dimensional pitching dynamic stiffness for $\alpha = 0{\cdot}01$ ($d/a_0 = 0{\cdot}25$)

n, m	$\frac{\omega a_0}{\mathrm{Re}(c_s)} = 0{\cdot}014273$	$\frac{\omega a_0}{\mathrm{Re}(c_s)} = 4{\cdot}2819$	$\frac{\omega a_0}{\mathrm{Re}(c_s)} = 10{\cdot}2509$
$\leqslant 1$	3·4062 − 0·02457i	5·3957 + 2·7380i	5·0558 + 6·1451i
$\leqslant 2$	3·4094 − 0·02462i	5·3963 + 2·7393i	5·0563 + 6·1454i
$\leqslant 3$	3·4109 − 0·02465i	5·3953 + 2·7386i	5·0556 + 6·1460i
$\leqslant 4$	3·4114 − 0·02466i	5·3969 + 2·7389i	5·0560 + 6·1459i

and 10. Similar results for pitching motion are shown in Tables IV–VI. From these tables and other comparisons, one can observe that the differences between the cases $n, m \leqslant 3$ and the cases $n, m \leqslant 4$ are less than 1 per cent for most results. Therefore, it is assumed that the contribution from higher Fourier components is insignificant, and it is concluded that only two Fourier components ($n, m = 0$ and 1) for each foundation are enough for the cases of non-dimensional frequency up to 10 and non-dimensional foundation rigidity down to 0·01. And it is believed that the error for dynamic stiffness would be conservatively estimated less than 5 per cent for the cases of interest.

Since foundation stiffness has only a little influence on some dynamic stiffness functions (e.g. horizontal and torsional dynamic stiffness) unless the foundation stiffness is very small, say $\alpha \leqslant 0{\cdot}01$, some selected results are shown in Figures 2–10 for the case $d/a_0 = 0{\cdot}1$, which means the two foundations are very close. Also, Figure 11 shows some results for $d/a_0 = 1{\cdot}0$ and Figures 12 and 13 show the effect of the separation distance of the two foundations.

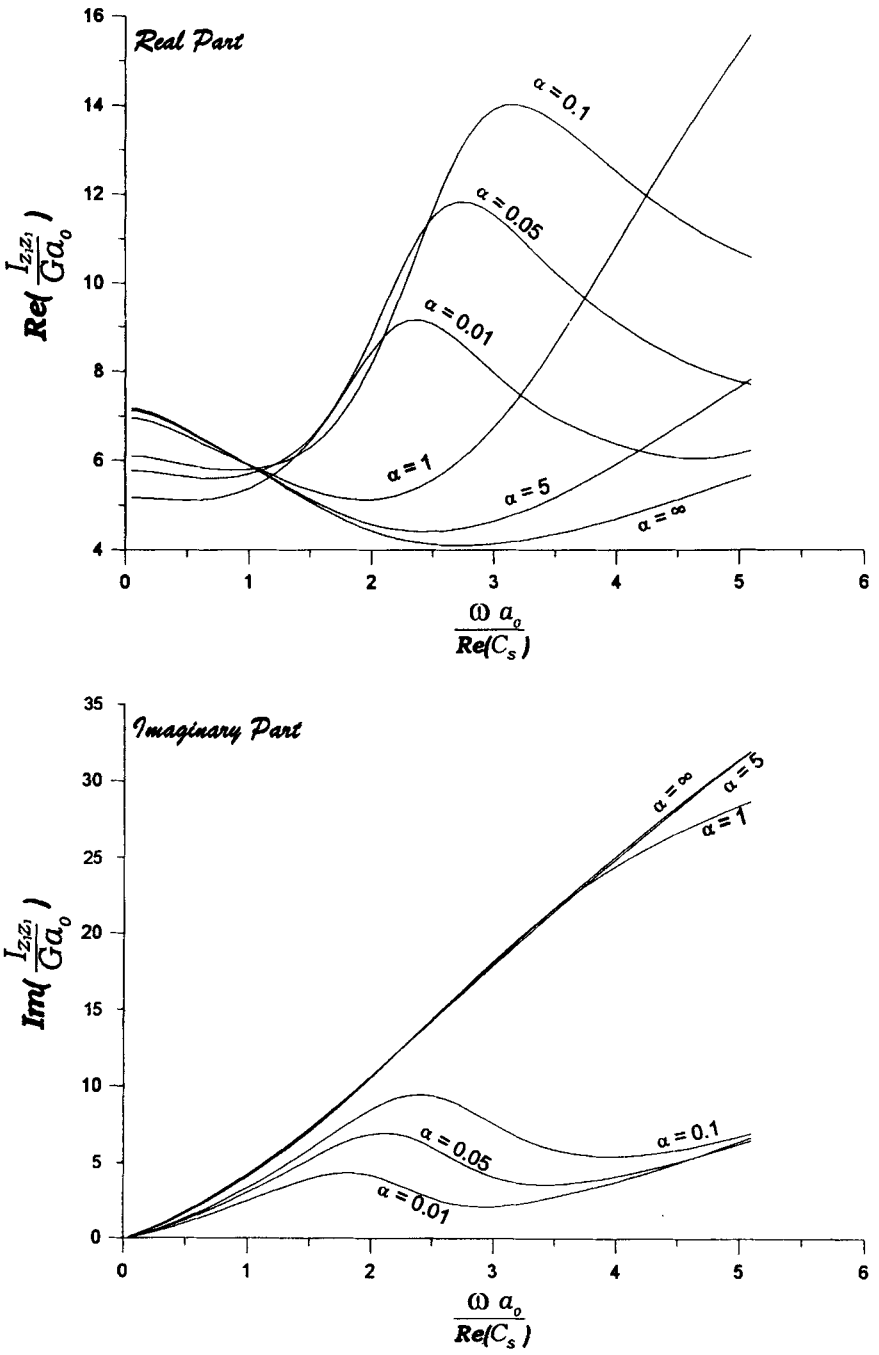

Figure 2. Non-dimensional vertical dynamic stiffness ($d/a_0 = 0{\cdot}1$)

Figure 2 shows the non-dimensional dynamic stiffness for the vertical motion of one foundation. From the figure, one can observe that the peak value of the real part of the dynamic stiffness function becomes larger and the corresponding frequency for the peak value becomes higher too, as the foundation plate becomes stiffer. For the imaginary part of the dynamic stiffness, one can see that it becomes smaller as the foundation becomes more flexible. Also, by comparing the curve for $\alpha = \infty$ in Figure 2 with the corresponding results in Reference 11 (Figure 4), one can observe that both results are reasonable and compatible. Figure 3 presents

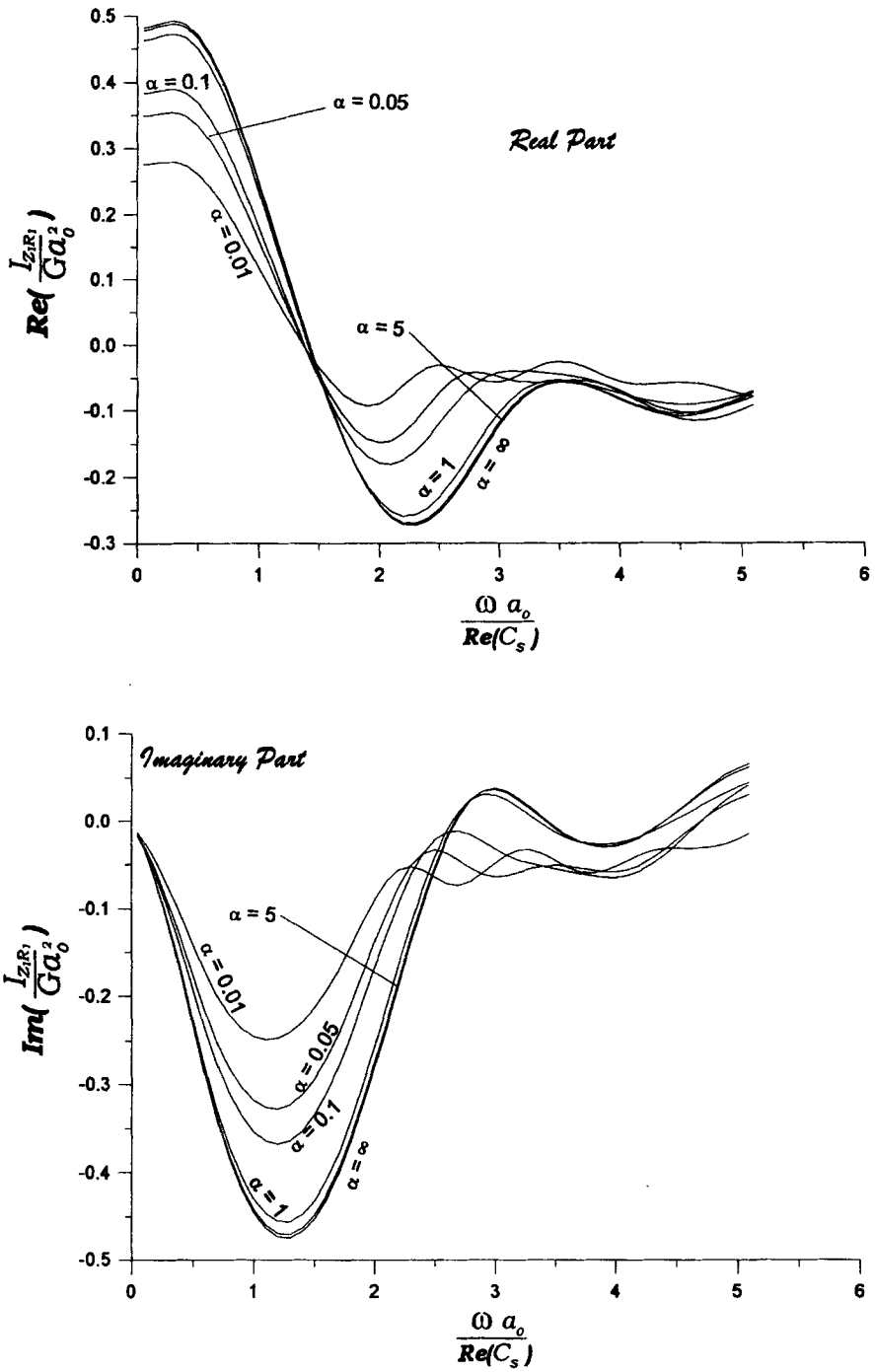

Figure 3. Non-dimensional coupling dynamic stiffness for vertical and rocking motions ($d/a_0 = 0{\cdot}1$)

the non-dimensional coupling dynamic stiffness for vertical and rocking motions of one foundation. From this figure, one can see that most coupling between the two motions occurs in the non-dimensional frequency range 0–3. One should also note that this coupling will not occur for a single foundation case. Figure 4 gives the non-dimensional coupling dynamic stiffness for vertical motion of one foundation and rocking motion of

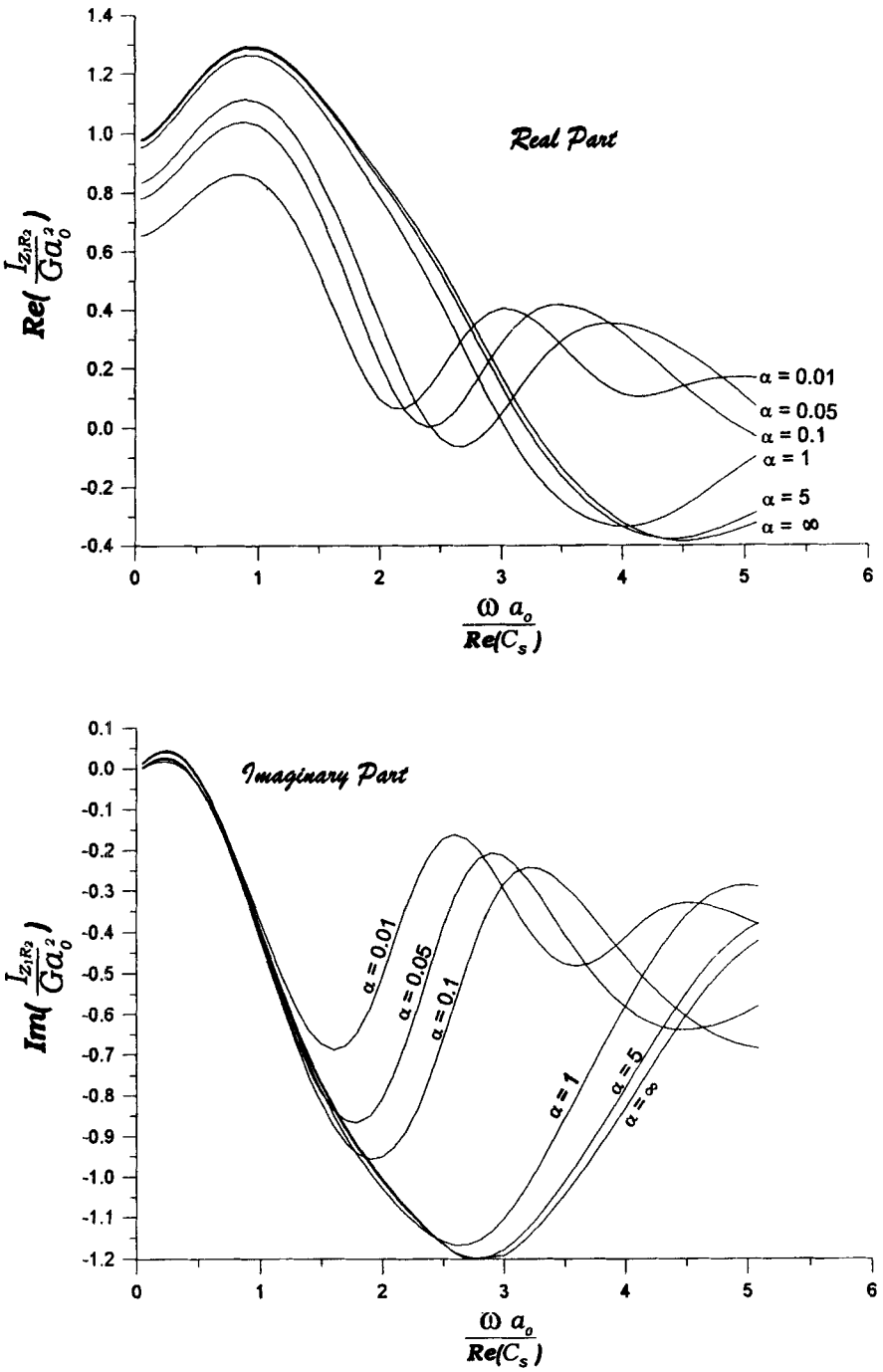

Figure 4. Non-dimensional coupling dynamic stiffness for vertical and rocking motions ($d/a_0 = 0{\cdot}1$)

another foundation. Comparing this figure with Figure 3, one observes that the coupling phenomenon shown in Figure 4 is even stronger than that shown in Figure 3. This is because the coupling shown in Figure 3 is due to the existence of the other foundation which scatters back the waves generated by the vertical vibration of the foundation.

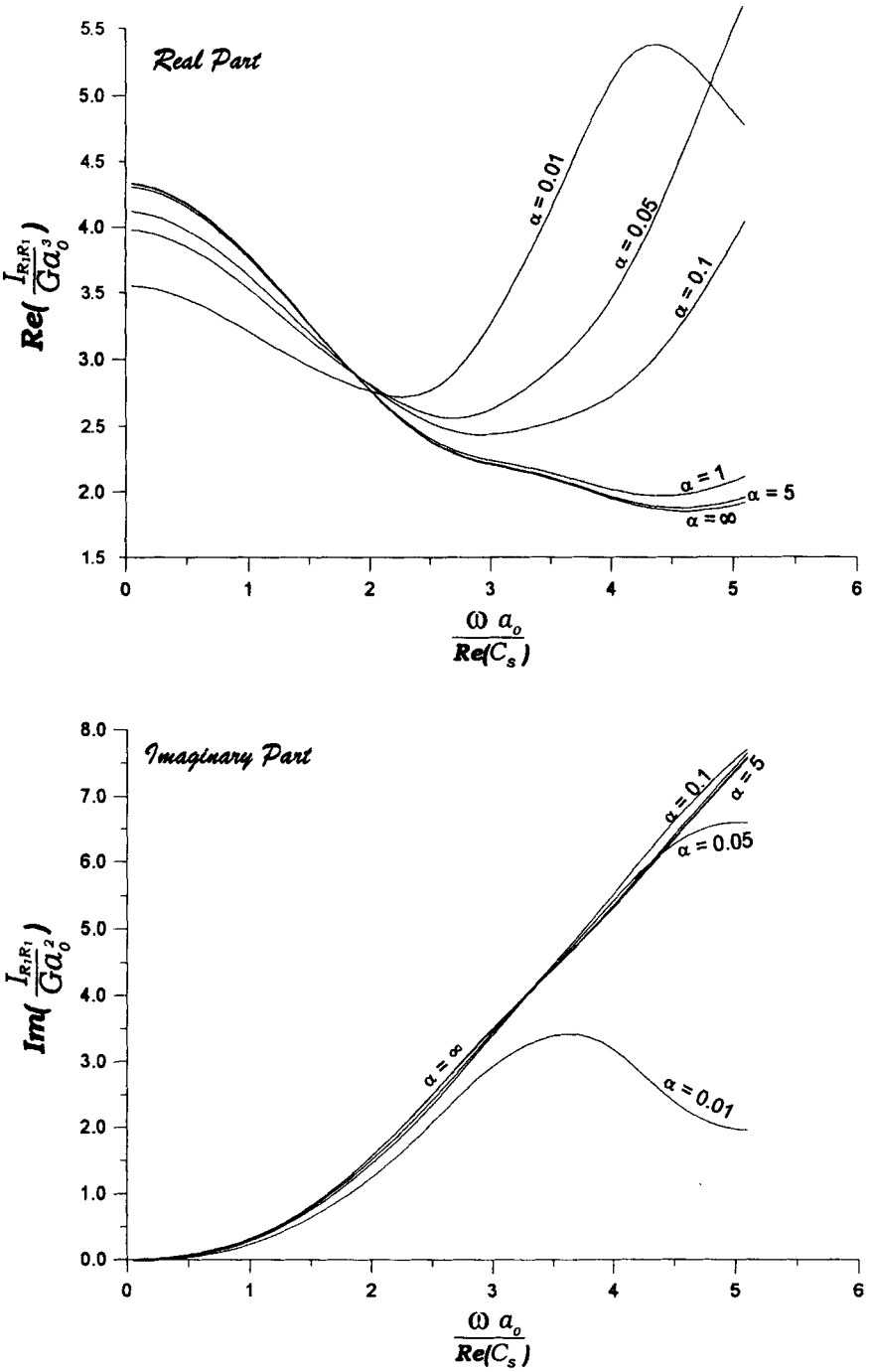

Figure 5. Non-dimensional rocking dynamic stiffness ($d/a_0 = 0{\cdot}1$)

Figures 5 and 6 show the non-dimensional dynamic stiffnesses for rocking and pitching motions of one foundation respectively. Comparing the two figures, one can see that the two dynamic stiffnesses become identical when the frequency goes higher, and this trend occurs earlier at a lower frequency as the stiffness of the foundation become smaller. These two dynamic stiffnesses should be identical for the case of only a single

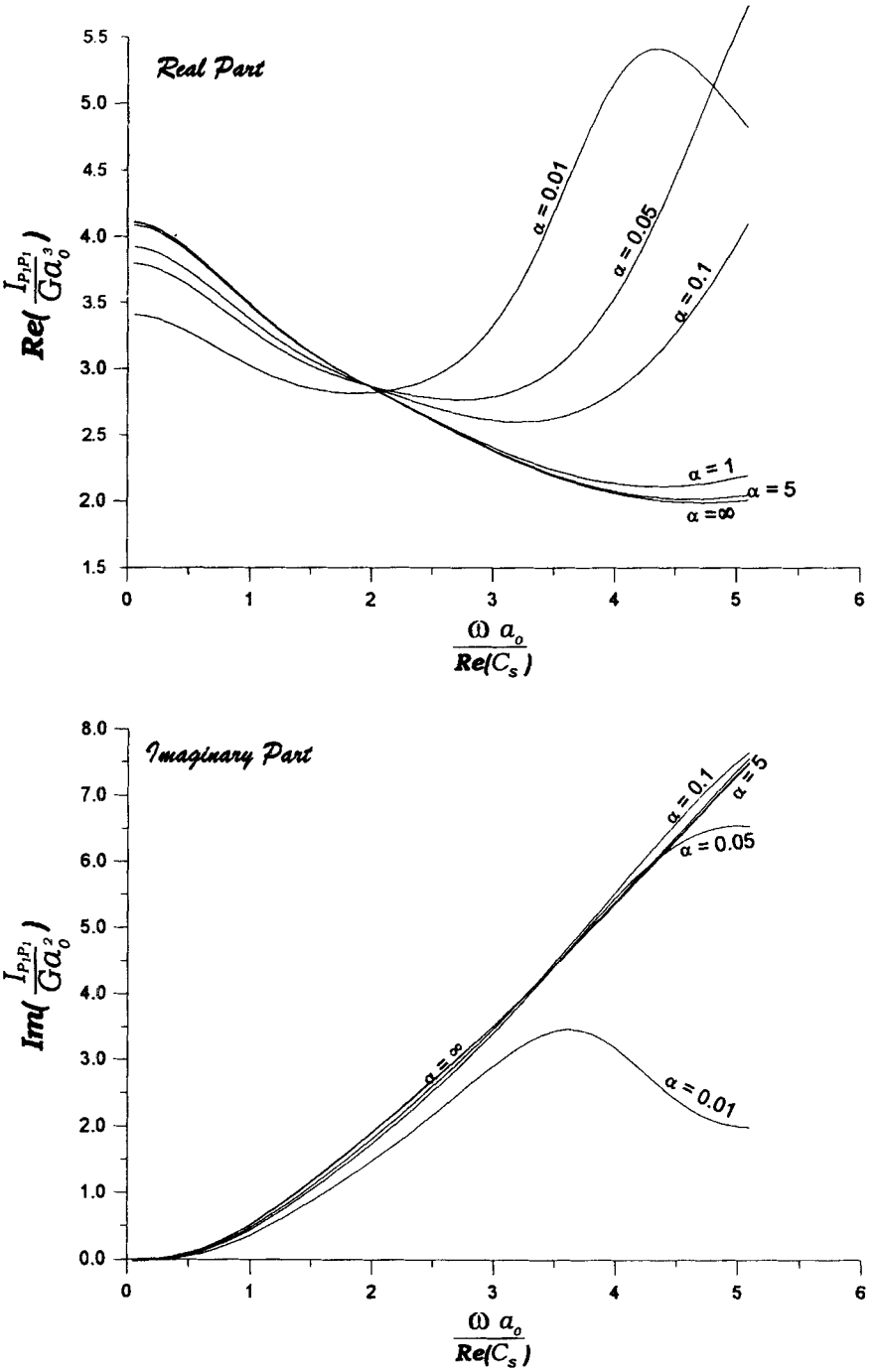

Figure 6. Non-dimensional pitching dynamic stiffness ($d/a_0 = 0{\cdot}1$)

foundation. The reason for this phenomenon is that the higher damping effect for the higher frequency wave (i.e. shorter wavelength) makes the interaction phenomenon of two foundations diminish as the excitation frequency goes up. Also, as the foundation stiffness goes down, the interaction effect of two foundations becomes less. This phenomenon can be observed in Figure 2 too. Again, by comparing the curves for $\alpha = \infty$

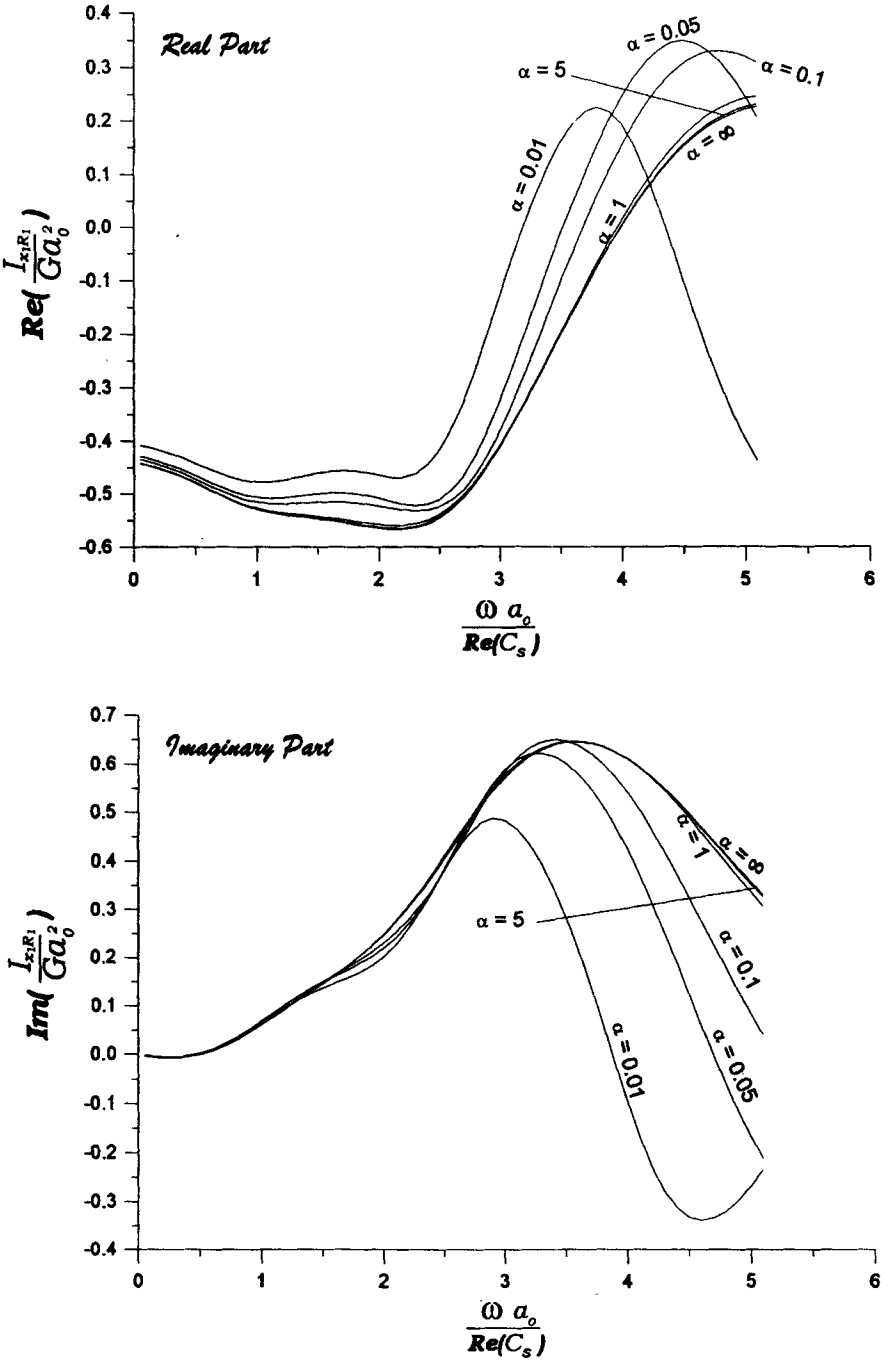

Figure 7. Non-dimensional coupling dynamic stiffness for horizontal and rocking motions ($d/a_0 = 0{\cdot}1$)

in Figures 5 and 6 with the corresponding results in Reference 11 (Figure 6), one can also observe similarity. This proves that both results are reasonable. Figures 7 and 8 show the non-dimensional coupling dynamic stiffness for rocking and horizontal (x-direction) motions of one foundation and the non-dimensional coupling dynamic stiffness for pitching and horizontal (y-direction) motions of one foundation respectively. From these figures, one can also observe the similar trend as indicated in Figures 5 and 6, except this trend

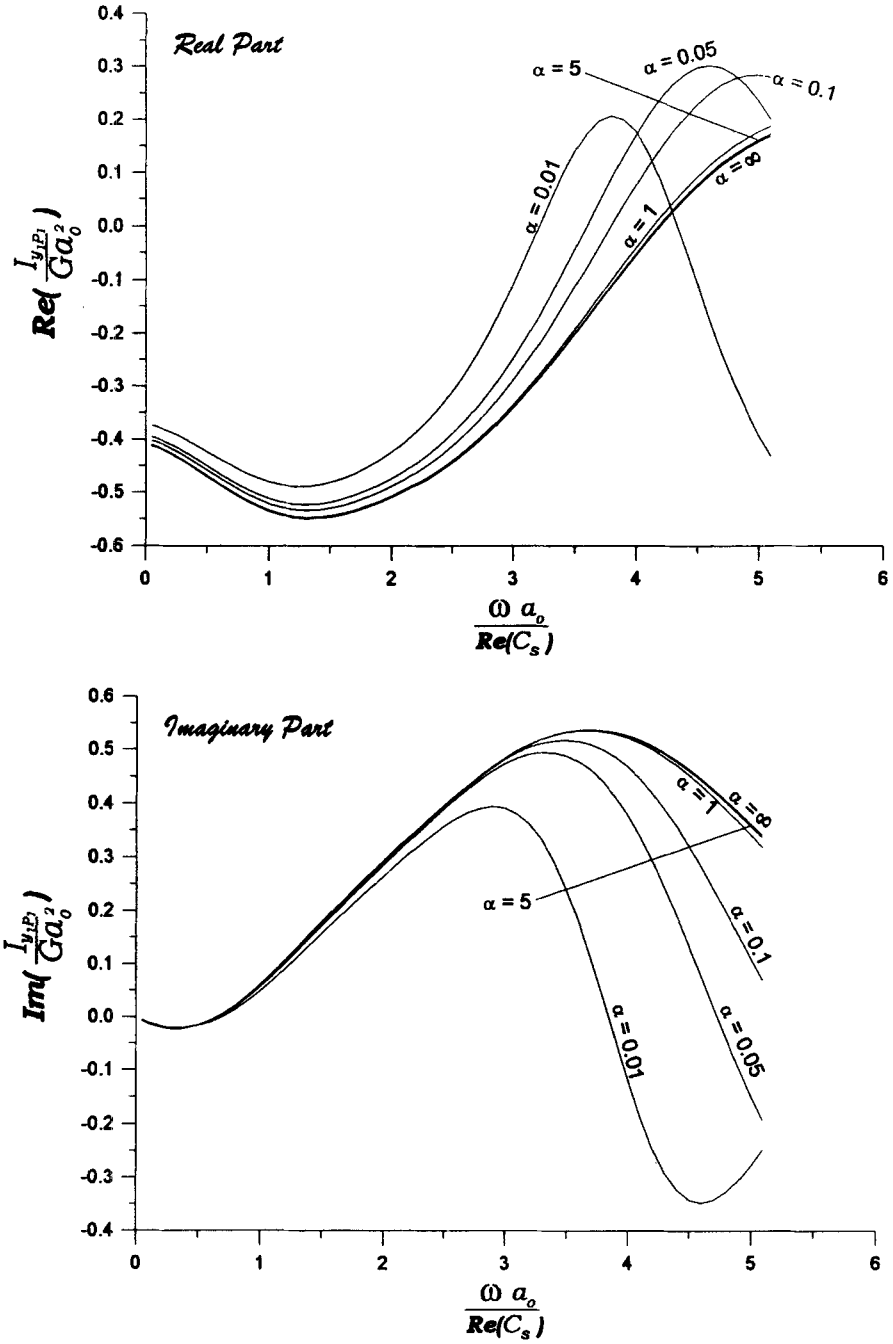

Figure 8. Non-dimensional coupling dynamic stiffness for horizontal and pitching motions ($d/a_0 = 0{\cdot}1$)

occurs from a higher frequency in Figures 7 and 8 than that in Figures 5 and 6. Figures 9 and 10 show the non-dimensional coupling dynamic stiffness for two rocking motions of two foundations and the non-dimensional coupling dynamic stiffness for two pitching motions of two foundations, respectively. Comparing these two figures, one can see that the two coupling behaviours are different and the coupling of the two rocking motions seems stronger than that of the two pitching motions. Also, the flexibility effect on the coupling dynamic stiffness for the two pitching motions is weaker.

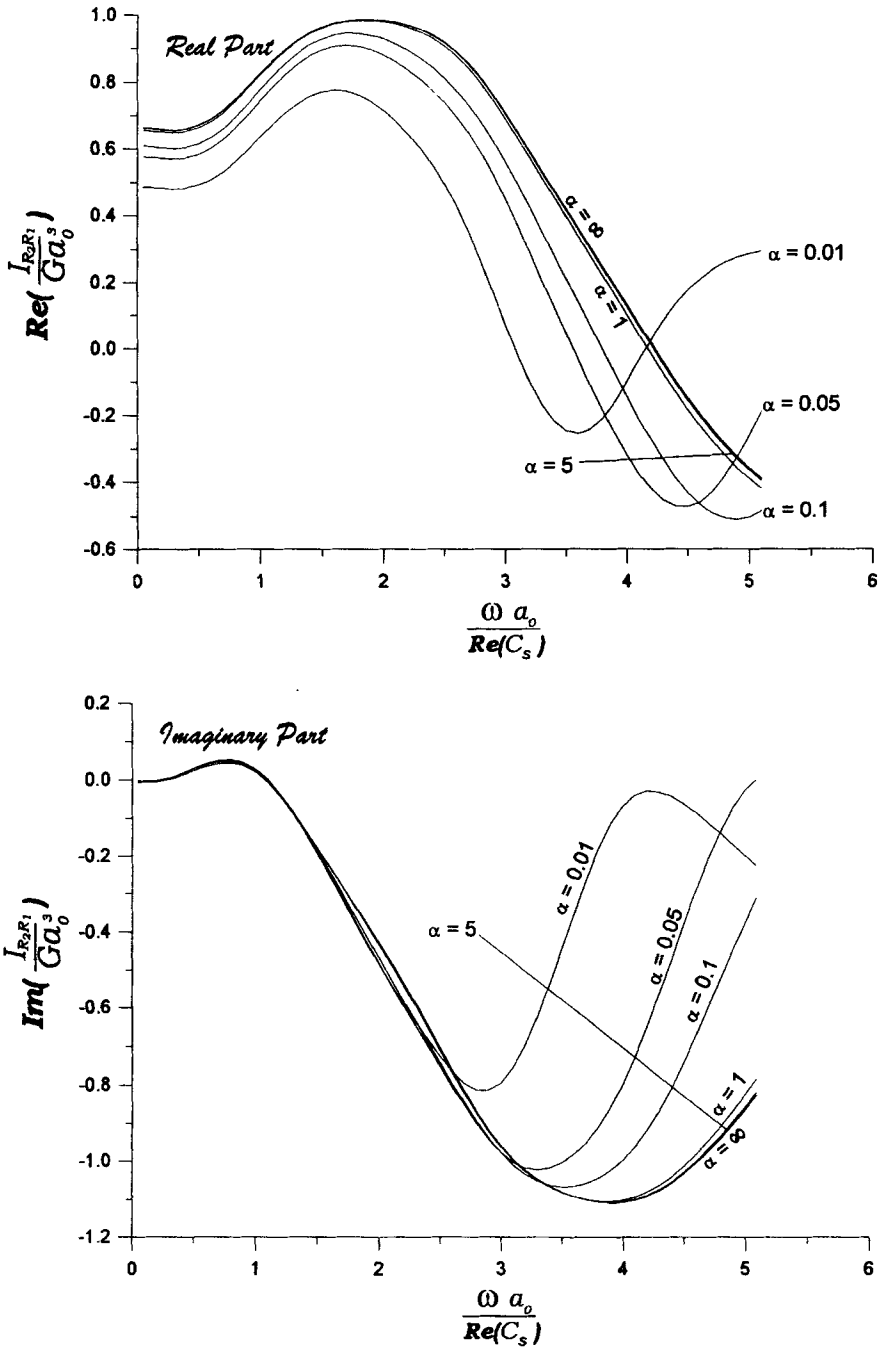

Figure 9. Non-dimensional coupling dynamic stiffness for two rocking motions ($d/a_0 = 0{\cdot}1$)

Figure 11 shows some numerical results of non-dimensional dynamic stiffness of vertical motion for the case of $d/a_0 = 1{\cdot}0$. By comparing with Figure 2, one can see a similar pattern of the effect due to foundation stiffness. Also, one can observe that when the non-dimensional frequency is greater than a certain value, the dynamic stiffnesses for both cases $d/a_0 = 0{\cdot}1$ and $1{\cdot}0$ are almost identical. The reason for this phenomenon is that a higher excitation frequency will cause a higher damping effect for the interaction of two foundations as

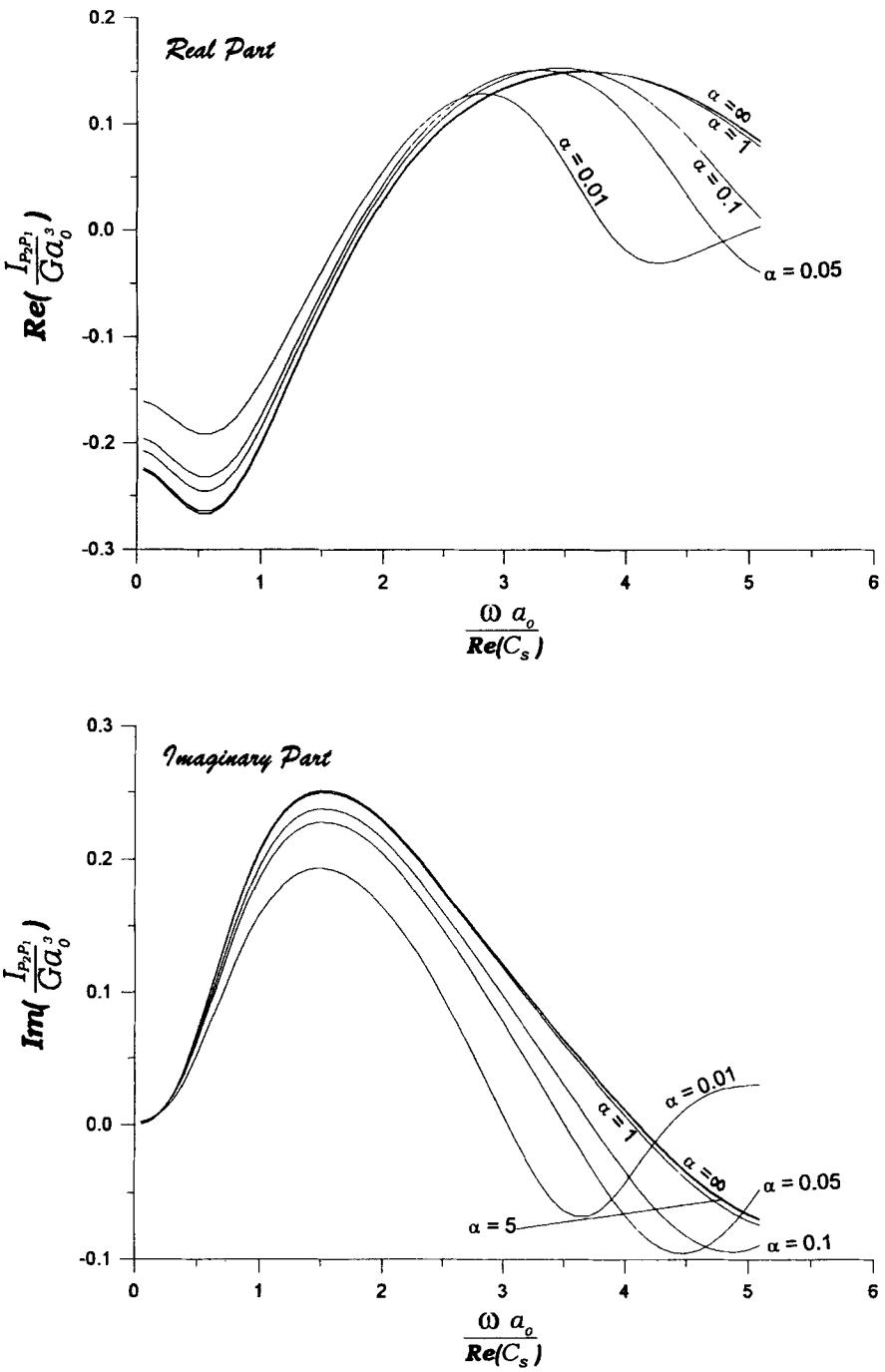

Figure 10. Non-dimensional coupling dynamic stiffness for two pitching motions ($d/a_0 = 0{\cdot}1$)

stated before. This means that when excitation is greater than a certain value, no interaction between the two foundations will be observed at all. Also, as the foundations become stiffer, the magnitude of this non-interaction frequency value becomes greater. For example, these values are about 3·0 for $\alpha = \infty$, 2·0 for $\alpha = 0{\cdot}1$ and 1·1 for $\alpha = 0{\cdot}01$. This is because the interaction effect becomes greater as the foundations become stiffer.

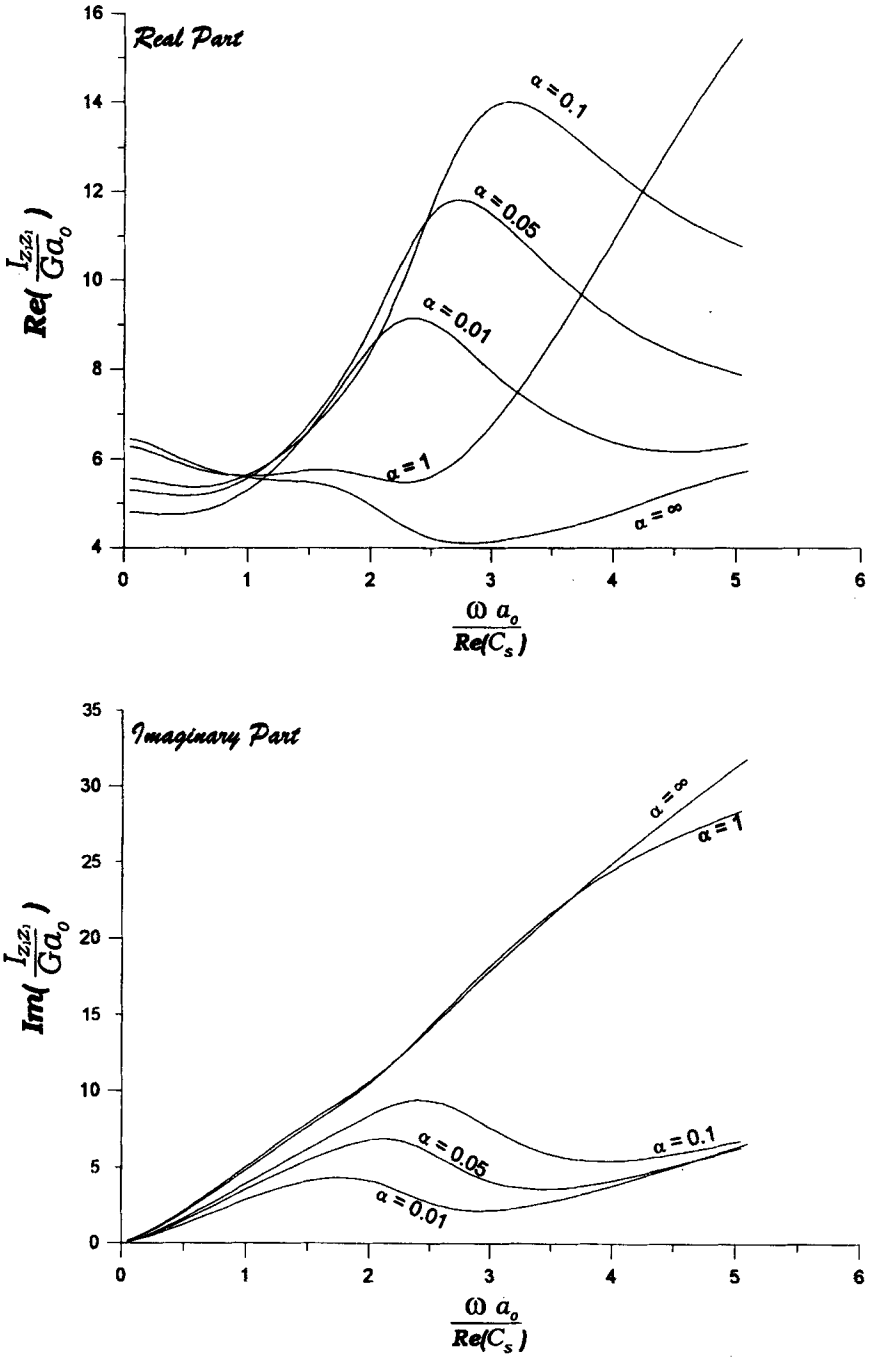

Figure 11. Non-dimensional vertical dynamic stiffness ($d/a_0 = 1{\cdot}0$)

Figures 12 and 13 show the coupling dynamic stiffnesses for vertical motions of the two foundations and horizontal motions (y-direction) of the two foundations respectively. For the figures, the non-dimensional stiffness parameter of the foundations (α) is 0·1 and the non-dimensional separation distances (d/a_0) of the two foundations are 0·1, 1·0, 5·0, 10·0 and ∞. By observing these two figures, one can find the coupling effect diminishes as the separation distance of the two foundations becomes greater, and also the coupling effect

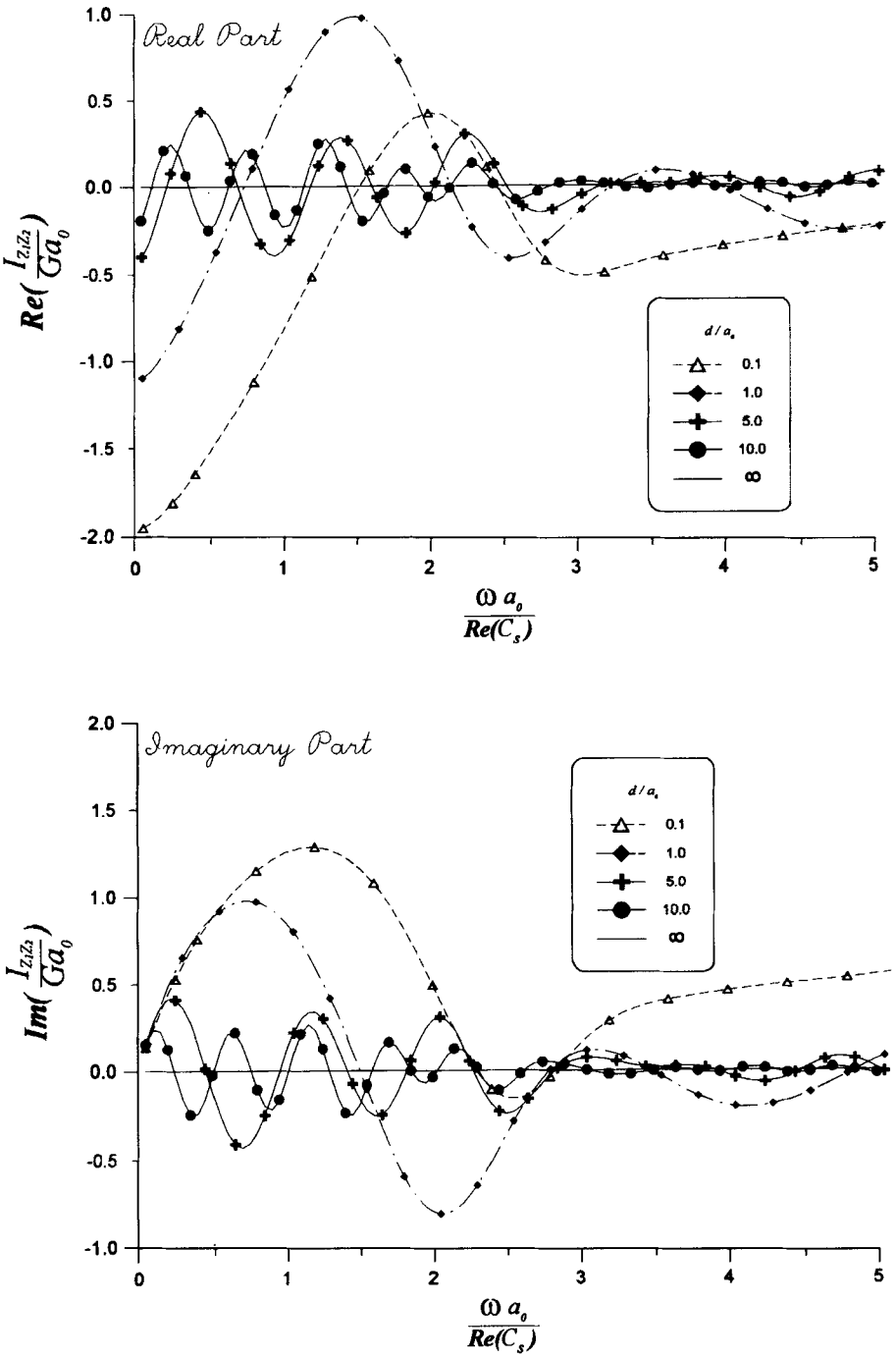

Figure 12. Non-dimensional coupling dynamic stiffness for two vertical motions ($\alpha = 0{\cdot}1$)

decays as the excitation frequency goes up. This is because of the damping effect of the soil medium. Also, one can observe some oscillation of the coupling dynamic stiffnesses along the zero axis which is for the case of $\alpha = \infty$. By comparing these two figures, one can see that the period of the oscillation for the coupling vertical dynamic stiffness is shorter. The reason for this phenomenon is that the waves generated by vertical motion are dominated by P-waves, and the waves generated by horizontal motion are dominated by S-waves.

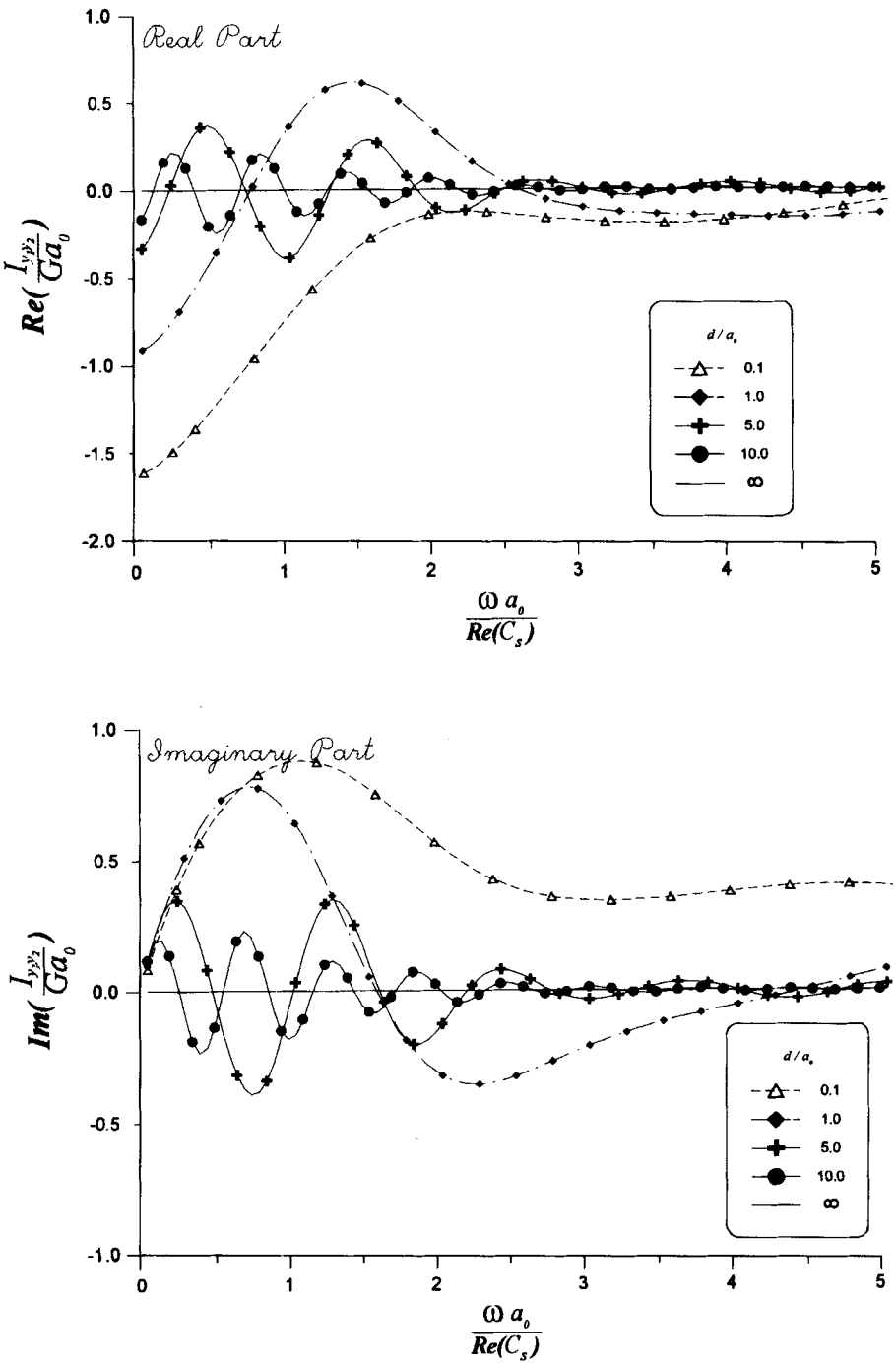

Figure 13. Non-dimensional coupling dynamic stiffness for two horizontal motions ($\alpha = 0{\cdot}1$)

CONCLUSIONS AND DISCUSSION

In the above numerical examples, the boundary condition at the rims of the foundations is assumed to be hinged. For other boundary conditions, the procedure developed in the paper can also be employed. Apparently, the flexibility effect on the dynamic stiffnesses will be different for other boundary conditions.

For example, if a clamped (fixed) condition is assumed at the rims of the foundations, the flexibility effect will be less. This is because more constraint at the rims of the foundations will increase the overall rigidity of the foundations. In other words, this constraint will make the foundations more resistable to deformation.

Although in the paper the boundary condition and excitation of foundation plates are assumed at the rims of the foundation plates, the dynamic stiffness functions for the cases of the boundary conditions and excitations described at other locations can also be obtained easily as long as all the foundation plates are axially symmetric; e.g. annular plates and circular plates with rigid cores.

After some extensive numerical investigations have been performed, one can conclude that, in general, the interaction of two foundations could be more dramatic if the rigidity of the foundations becomes higher. However, one should bear in mind that the interaction effect is strongly governed by excitation frequency too. Also, if the non-dimensional stiffness parameter of the foundation plates, α, is greater than 10, only a little flexibility effect is observed for a non-dimensional frequency up to 5. This means that the foundations can be treated as rigid foundations. When comparing the results with those for the case of a single foundation, one can also conclude that the flexibility effect for the two-foundation system is stronger than that for a single-foundation system. In addition, the inertial force of the flexible foundations may be important, since it could change the deformation shape of the flexible foundations during the vibration of the foundations. However, the inertial effect is neglected in the formulation in the paper. Hence, a further study about the effect of the inertial forces of the foundations themselves on the concerned dynamic stiffness matrix is necessary.

ACKNOWLEDGEMENTS

This work was sponsored by National Science Council of Taiwan under Contract No. NSC82-0115-E009-435. The support is greatly appreciated. The author would also like to express appreciation to Professor G.B. Warburton for his critical comments which made this paper more readable.

APPENDIX

The piecewise linear distribution of the tractions in the r-direction can be expressed as follows:

$$\begin{aligned}
\tau_{r_1 z_1, n} &= \sum_{j=1}^{m_1 - 1} h_j(r_1) q_j + h_0(r_1) q_0 + h_{m_1}(r_1) q_{m_1} = \mathbf{h}^{\mathrm{T}} \mathbf{q} \\
\sigma_{z_1 z_1, n} &= \sum_{j=1}^{m_1 - 1} h_j(r_1) p_j + h_0(r_1) p_0 + h_{m_1}(r_1) p_{m_1} = \mathbf{h}^{\mathrm{T}} \mathbf{p} \\
\tau_{\theta_1 z_1, n} &= \sum_{j=1}^{m_1 - 1} h_j(r_1) s_j + h_0(r_1) s_0 + h_{m_1}(r_1) s_{m_1} = \mathbf{h}^{\mathrm{T}} \mathbf{s}
\end{aligned} \tag{30}$$

or

$$\mathbf{t}_{1,n}(r_1) = \mathbf{H}_1^{\mathrm{T}} \mathbf{P}_{1,n} \tag{30a}$$

where

$$h_j(r_1) = \begin{cases} 1 + \dfrac{r_1 - r_{1,j}}{r_{1,j} - r_{1,j-1}} & \text{if } r_{1,j-1} \leqslant r_1 \leqslant r_{1,j} \text{ and } 1 \leqslant j \leqslant m_1 \\ 1 - \dfrac{r_1 - r_{1,j}}{r_{1,j+1} - r_{1,j}} & \text{if } r_{1,j} \leqslant r_1 \leqslant r_{1,j+1} \text{ and } 0 \leqslant j \leqslant m_1 - 1 \\ 0 & \text{otherwise} \end{cases} \tag{31}$$

matrix $\mathbf{H}_1^{\mathrm{T}} = \mathrm{diag}[\mathbf{h}^{\mathrm{T}}, \mathbf{h}^{\mathrm{T}}, \mathbf{h}^{\mathrm{T}}]$, vector $\mathbf{P}_{1,n}^{\mathrm{T}} = (\mathbf{q}^{\mathrm{T}}, \mathbf{p}^{\mathrm{T}}, \mathbf{s}^{\mathrm{T}})$, and q_j, p_j and s_j are the stress intensities at nodal ring j for $\tau_{r_1 z_1, n}$, $\sigma_{z_1 z_1, n}$ and $\tau_{\theta_1 z_1, n}$ respectively. Vector $\mathbf{P}_{1,n}$ in equations (30) could be either $\mathbf{P}_{1,n}^{\mathrm{s}}$ or $\mathbf{P}_{1,n}^{\mathrm{a}}$ for symmetric or anti-symmetric Fourier components respectively, and subscripts n and $m_1 - 1$ represent the nth

Fourier component and the number of piecewise linear subdivision of the radius of foundation respectively. Matrix $\mathbf{H}_2^{\mathrm{T}}$ and vector $\mathbf{P}_{2,m}$ can be similarly defined.

The Bessel function matrix $\mathbf{J}_n$ can be written as

$$\mathbf{J}_n = \begin{bmatrix} J_n'(k_1 r_1) & 0 & \dfrac{n}{r_1} J_n(k_1 r_1) \\ 0 & k_1 J_n(k_1 r_1) & 0 \\ \dfrac{n}{r_1} J_n(k_1 r_1) & 0 & J_n'(k_1 r_1) \end{bmatrix} \tag{32}$$

where $J_n(k_1 r_1)$ is the first kind of Bessel function with order n, and $J_n'(k_1 r_1) = \mathrm{d}J_n(k_1 r_1)/\mathrm{d}r_1$.

The transfer matrix of the half-space medium $\mathbf{Q}$ can be expressed as

$$\mathbf{Q} = \begin{bmatrix} -\nu' k_\beta^2/\Lambda & k_1(2\nu\nu' - 2k_1^2 + k_\beta^2)/\Lambda & 0 \\ k_1(2\nu\nu' - 2k_1^2 + k_\beta^2)/\Lambda & -\nu k_\beta^2/\Lambda & 0 \\ 0 & 0 & -1/G\nu' \end{bmatrix} \tag{33}$$

where $\nu = (k_1^2 - \omega^2/c_{\mathrm{p}}^2)^{0.5}$, $\nu' = (k_1^2 - \omega^2/c_{\mathrm{s}}^2)^{0.5}$, $\Lambda = G[4k_1^2\nu\nu' - (2k_1^2 - k_\beta^2)^2]$, c_{p} is the compressional wave velocity, c_{s} is the shear wave velocity, and G is the complex shear modulus.

The matrix $\bar{\mathbf{D}}_n$ in equation (3) can be expressed as

$$\bar{\mathbf{D}}_n = \begin{bmatrix} (-\mathbf{D}_{n+1}^{\mathrm{T}} + \mathbf{D}_{n-1}^{\mathrm{T}})/2 & \mathbf{0} & (\mathbf{D}_{n+1}^{\mathrm{T}} + \mathbf{D}_{n-1}^{\mathrm{T}})/2 \\ \mathbf{0} & \mathbf{D}_n^{\mathrm{T}} & \mathbf{0} \\ (\mathbf{D}_{n+1}^{\mathrm{T}} + \mathbf{D}_{n-1}^{\mathrm{T}})/2 & \mathbf{0} & (-\mathbf{D}_{n+1}^{\mathrm{T}} + \mathbf{D}_{n-1}^{\mathrm{T}})/2 \end{bmatrix} \tag{34}$$

where

$$\mathbf{D}_{n+1}^{\mathrm{T}} = \int_0^{a_1} r_1 J_{n+1}(k_1 r_1)\mathbf{h}^{\mathrm{T}}\,\mathrm{d}r_1 \tag{34a}$$

$$\mathbf{D}_n^{\mathrm{T}} = \int_0^{a_1} r_1 J_n(k_1 r_1)\mathbf{h}^{\mathrm{T}}\,\mathrm{d}r_1 \tag{34b}$$

$$\mathbf{D}_{n-1}^{\mathrm{T}} = \int_0^{a_1} r_1 J_{n-1}(k_1 r_1)\mathbf{h}^{\mathrm{T}}\,\mathrm{d}r_1 \tag{34c}$$

One should note that the vectors $\mathbf{D}_{n+1}^{\mathrm{T}}$, $\mathbf{D}_n^{\mathrm{T}}$ and $\mathbf{D}_{n-1}^{\mathrm{T}}$ are Hankel transforms of the vector $\mathbf{h}^{\mathrm{T}}$ defined in equations (30).

The influence matrices shown in equation (8c) are defined as follows:

$$\mathbf{K}_{nn}^{\mathrm{s}} = \int_0^{\infty}\int_0^{a_1}\int_0^{2\pi} \mathbf{H}_1 \mathbf{L}_n^{\mathrm{s}} \mathbf{L}_n^{\mathrm{s}} \mathbf{J}_n r_1\,\mathrm{d}\theta_1\,\mathrm{d}r_1\,\mathbf{Q}\bar{\mathbf{D}}_n\,\mathrm{d}k_1 \tag{35a}$$

$$\mathbf{K}_{nn}^{\mathrm{a}} = \int_0^{\infty}\int_0^{a_1}\int_0^{2\pi} \mathbf{H}_1 \mathbf{L}_n^{\mathrm{a}} \mathbf{L}_n^{\mathrm{a}} \mathbf{J}_n r_1\,\mathrm{d}\theta_1\,\mathrm{d}r_1\,\mathbf{Q}\bar{\mathbf{D}}_n\,\mathrm{d}k_1 \tag{35b}$$

$$\mathbf{K}_{n,m}^{\mathrm{s}} = \int_0^{\infty}\int_0^{a_1}\int_0^{2\pi} \mathbf{H}_1 \mathbf{L}_n^{\mathrm{s}} \bar{\mathbf{T}} \bar{\mathbf{L}}_m^{\mathrm{s}} \bar{\mathbf{J}}_m r_1\,\mathrm{d}\theta_1\,\mathrm{d}r_1\,\bar{\mathbf{Q}}\bar{\mathbf{D}}_m\,\mathrm{d}k_2 \tag{36a}$$

$$\mathbf{K}_{n,m}^{\mathrm{a}} = \int_0^{\infty}\int_0^{a_1}\int_0^{2\pi} \mathbf{H}_1 \mathbf{L}_n^{\mathrm{a}} \bar{\mathbf{T}} \bar{\mathbf{L}}_m^{\mathrm{a}} \bar{\mathbf{J}}_m r_1\,\mathrm{d}\theta_1\,\mathrm{d}r_1\,\bar{\mathbf{Q}}\bar{\mathbf{D}}_m\,\mathrm{d}k_2 \tag{36b}$$

$$\bar{\mathbf{K}}^{s}_{mm} = \int_0^{\infty}\int_0^{a_2}\int_0^{2\pi} \mathbf{H}_2\bar{\mathbf{L}}^{s}_{m}\bar{\mathbf{L}}^{s}_{m}\bar{\mathbf{J}}_m r_2\,\mathrm{d}\theta_2\,\mathrm{d}r_2\,\bar{\mathbf{Q}}\bar{\mathbf{D}}_m\,\mathrm{d}k_2 \tag{37a}$$

$$\bar{\mathbf{K}}^{a}_{mm} = \int_0^{\infty}\int_0^{a_2}\int_0^{2\pi} \mathbf{H}_2\bar{\mathbf{L}}^{a}_{m}\bar{\mathbf{L}}^{a}_{m}\bar{\mathbf{J}}_m r_2\,\mathrm{d}\theta_2\,\mathrm{d}r_2\,\bar{\mathbf{Q}}\bar{\mathbf{D}}_m\,\mathrm{d}k_2 \tag{37b}$$

$$\bar{\mathbf{K}}^{s}_{m,n} = \int_0^{\infty}\int_0^{a_2}\int_0^{2\pi} \mathbf{H}_2\bar{\mathbf{L}}^{s}_{m}\bar{\mathbf{T}}^{\mathrm{T}}\mathbf{L}^{s}_{n}\mathbf{J}_n r_2\,\mathrm{d}\theta_2\,\mathrm{d}r_2\,\mathbf{Q}\mathbf{D}_n\,\mathrm{d}k_1 \tag{38a}$$

$$\bar{\mathbf{K}}^{a}_{m,n} = \int_0^{\infty}\int_0^{a_2}\int_0^{2\pi} \mathbf{H}_2\bar{\mathbf{L}}^{a}_{m}\bar{\mathbf{T}}^{\mathrm{T}}\mathbf{L}^{a}_{n}\mathbf{J}_n r_2\,\mathrm{d}\theta_2\,\mathrm{d}r_2\,\mathbf{Q}\mathbf{D}_n\,\mathrm{d}k_1 \tag{38b}$$

REFERENCES

1. G. B. Warburton, J. D. Richardson and J. J. Webster, 'Harmonic response of masses on an elastic half-space', *J. eng. ind. trans. ASME* **94**, 193–200 (1972).
2. S. Savidis and T. Richter, 'Dynamic interaction of rigid foundations', *Proc. IX int. conf. soil mech. found. eng.*, Tokyo, 1977, pp. 369–374.
3. H. L. Wong and J. E. Luco, 'Dynamic interaction between rigid foundations in a layered half-space', *Soil dyn. earthquake eng.* **5**, 149–158 (1986).
4. Th. Triantafyllidis and B. Prange, 'Dynamic subsoil-coupling between rigid, circular foundations on the halfspace', *Soil dyn. earthquake eng.* **8**, 9–21 (1989).
5. H.-T. Lin, J. M. Roesset and J. L. Tassoulas, 'Dynamic interaction between adjacent foundations', *Earthquake eng. struct. dyn.* **15**, 323–343 (1987).
6. H. Kawakami and S. Tasaki, 'Soil–structure interaction of rigid structures considering through-soil coupling between adjacent structures', *Proc. 9th world conf. earthquake eng.*, Tokyo-Kyoto, Japan, Vol. III, 1988, pp. 385–390.
7. S. Krenk and H. Schmidt, 'Vibration of an elastic circular plate on an elastic half space — a direct approach', *J. appl. mech. ASME* **48**, 161–168 (1981).
8. M. Iguchi and J. E. Luco, 'Vibration of flexible plate on viscoelastic medium', *J. eng. mech. div. ASCE* **108**, 1103–1120 (1982).
9. R. K. N. D. Rajapakse, 'Dynamic response of elastic plates on viscoelastic half space', *J. eng. mech. div. ASCE* **115**, 1867–1881 (1989).
10. G. S. Liou and P. H. Huang, 'Effect of flexibility on impedance functions for circular foundation', *J. eng. mech. ASCE* **120**, 1429–1446 (1994).
11. G. S. Liou, 'Dynamic stiffness matrices for two circular foundations', *Earthquake eng. struct. dyn.* **23**, 193–210 (1994).